AIAA 82-4079

Constrained and Unconstrained Modes: Some Modeling Aspects of Flexible Spacecraft

Hari B. Hablani*
Purdue University, West Lafayette, Ind.

Spacecraft that are partially rigid and partially flexible may be dynamically modeled in terms of either "constrained" modes of vibration, for which the rigid part is held motionless, or the "unconstrained" modes of the whole vehicle. A model "completeness index" is defined for each expansion and used as a truncation criterion. Using as an example a large flexible platform with a rigid body at the center, it is shown that as the rigid portion of the vehicle becomes very small, a great many constrained modes are needed to achieve satisfactory model completeness. Otherwise, one finds an erroneous distribution of angular momentum among the modes. It is also shown that the importance of unconstrained modes is not necessarily ordered by frequency.

Nomenclature

D = flexural rigidity of $\mathcal{E}$
I_{rx}, I_{ry} = principal moments of inertia of $\mathcal{R}$ about the x and y axis, respectively
I_{ex}, I_{ey} = principal moments of inertia of $\mathcal{E}$ about the x and y axis, respectively
I_{xx}, I_{yy} = principal moments of inertia of $\mathcal{V}$ about the x and y axis, respectively
N = number of constrained or unconstrained elastic modes
N_e = number of finite elements in the x and y directions = 4
U_n, Q_n = nth constrained mode and the associated modal coordinate
$a,b;a',b'$ = length and width of $\mathcal{E}$: $a'=a/N_e$, $b'=b/N_e$
m, m_r, m_e = masses of $\mathcal{V}$, $\mathcal{R}$, and $\mathcal{E}$, respectively
$oxyz$ = inertial triad: ox = longitudinal axis, oy = transverse axis, oz = normal axis; also principal coordinate system when $\mathcal{V}$ is undisturbed
p, h_x, h_y = linear and angular momentum of $\mathcal{V}$ about the z, x, and y axis, respectively
$\hat{p}_\alpha, \hat{h}_{x\alpha}, \hat{h}_{y\alpha}$ = the normalized p_α, $h_{x\alpha}$, $h_{y\alpha}$, $\alpha \in \mathcal{S}_e$
q = vector of nodal variables
t = time
$u(x,y,t)$ = deformation of any point $P \in \mathcal{E}$ in the rigid-body-embedded-triad
$w(x,y,t)$ = displacement of any point $P \in \mathcal{V}$ in the inertial triad
z_c = translational motion of $\mathcal{R}$ along the z axis
$z_{c\alpha}$ = rectilinear motion of $\mathcal{R}$ along the z axis during the mode $w_\alpha(x,y)$
$\mathcal{K}, \mathcal{M}$ = stiffness and mass matrix
$\mathcal{R}^n$, $\mathcal{R}^{n\times m}$ = an n-column vector and an $n \times m$ matrix in real Euclidean space
$\mathcal{S}, \mathcal{S}_e$ = sequence (1,2,...) and (4,5,...), respectively
$\mathcal{S}_N, \mathcal{S}_{eN}$ = sequence (1,...,N) and (4,...,N+3), respectively
$\bar{\mathcal{S}}, \bar{\mathcal{S}}_e$ = sequence (1,...,97) and (4,...,100), respectively
Ω_n = frequency of nth constrained mode
θ_x, θ_y = rotation of $\mathcal{R}$ about the x and y axis, respectively
$\theta_{x\alpha}, \theta_{y\alpha}$ = rotation of $\mathcal{R}$ about the x and y axis during αth unconstrained mode
μ = mass/area of $\mathcal{E}$
ν = Poisson's ratio of $\mathcal{E}$
μ_f = $\sqrt{\mu a' b'}$
σ = aspect ratio = a/b
$\tilde{\omega}_\alpha$ = nondimensional frequency
ω_α = frequency of αth unconstrained mode = $\tilde{\omega}_\alpha \sqrt{D/\mu a^4}$
$(\dot{})$ = temporal derivative
$(\hat{})$ = normalized value

I. Introduction

SINCE the naive days of Explorer I (1958) researchers and practicing engineers have brought a constellation of changes in their ability to fly, triumphantly, sophisticated space vehicles to far destinations. Yet, the physical complexity of the large space structures of the future is so extraordinary that the consequent modeling errors erode confidence in our capabilities.[1] This paper is devoted to improving, to a modest extent, our ability to model the dynamics and control of flexible spacecraft. Specifically, it is concerned with the vibrational interaction between different parts of a space vehicle or structure.

To establish a framework for our contribution a brief literature survey is in order. A typical existing spacecraft includes a rigid hub and elastic appendages. For vibrational analysis of such spacecraft a hierarchy of modes exist. For a clear understanding the reader will require the following terminology.

1) Constrained modes: In this situation the rigid hub is constrained to be motionless and the appendage vibrates. More common phrases such as "cantilever modes," "fixed-base modes," and "appendage modes" have the same meaning.

2) Unconstrained modes: In this case the entire vehicle vibrates and, in general, a motional interaction between various parts of the vehicle takes place. The term "vehicle mode" conveys the same meaning.

The above terminology is taken from Hughes.[2] We prefer the term "constrained modes" to "appendage modes" because many future space vehicles have nontopological tree configuration with re-entrant branches and closed loops of connectivity. Since almost the entire vehicle is flexible, the term "appendage" is misleading. Definitions similar to those above can be formulated for spinning or dual-spin spacecraft,

Received Oct. 30, 1979; revision received Dec. 30, 1980.

*Postdoctoral Research Scholar, School of Aeronautics and Astronautics; presently, NASA/NRC Associate at Johnson Space Center, Houston, Tex.

or for vehicles with control moment gyros. A more advanced family of modes in this hierarchy depends on controllers; however, these latter modes will not be discussed here in any detail. Intuition and literature suggest that, for a given order of discretization, accuracy of the vehicle dynamics improves as one migrates from the constrained modes to the unconstrained modes. Nonetheless, the unconstrained modes—probably the most accurate natural modes—have seldom been properly examined and characterized in the literature (the exceptions will be noted below). The above argument is based on the following observations.

The "hybrid coordinate approach" originated by Likins[3] affords an insight into dynamic behavior because he devises certain "flexibility influence coefficients" that are integrals of the constrained modes. Likins et al.[4] show that the coefficients are a measure of retainability of the constrained modes. This approach has received a wide recognition for simulation of complex spacecraft; Margulies et al.[5] offer a recent example. Nonetheless, the method does not characterize vehicle modes.

Hughes[2] describes general motion of spacecraft in terms of integrals of the constrained modes (similar to Likins[3]) and the unconstrained modes. Based on the integrals and the linear and angular momentum of the vehicle, Hughes[6] devises numerous "modal identities" between the vehicle inertia and the integrals. Characterization of the unconstrained modes by the integrals is one of the distinctive features of the dynamic analysis by Hughes. Thus, only recently has the interaction between rigid-body motion and structural deformation been theorized with a certain degree of preciseness.

It is noteworthy that if the spacecraft consists of relatively simple parts, rigid or elastic, and only interfacial variables are of concern, as in attitude control, then receptance or impedance of each part at the interface can be derived by continuum mechanics and the need for discretization eliminated altogether. Bishop and Johnson[7] and Poelaert[8,9] advocate the receptance method for such simple composite vehicles; the method is, of course, not restricted to spacecraft dynamics. Further, Poelaert[8,9] gives closed-form relations similar to a few of those by Hughes[2,6] for the case when discretization is in terms of assumed modes.

The primary intent of our studies is to implement the theory advanced by Hughes.[2,6] We compare accuracy of discretized models obtained by using the constrained modes and the unconstrained modes. Dependence of the rigid-body/structure interaction on their inertia ratios is examined in detail. A two-dimensional large space structure with a rigid body at the center is chosen for case study. The principal conclusion of this paper is that the vibrational interaction between the rigid body and the elastic structure depends crucially on their inertia ratios and is portrayed more accurately by the unconstrained modes (i.e., the vehicle modes). An important conclusion such as this should have been obvious from the beginning of spacecraft dynamics analysis, yet it has remained generally unnoticed. (See some discussion along these lines in Ref. 3, p. 69.)

II. Dynamics of a Two-Dimensional Large Space Structure

The space vehicle $\mathcal{V}$ (Fig. 1) can be regarded as a typical large space structure. It has a rectangular planform with no edge constraints and its neutral surface is planar. An equivalent distributed parameter model[10,11] is assumed to consist of a uniform elastic rectangular plate $\mathcal{E}$ and a rigid body $\mathcal{R}$ attached rigidly at the center of $\mathcal{E}$. Attitude control of $\mathcal{R}$, shape control of $\mathcal{E}$, and stationkeeping of $\mathcal{V}$ are contemplated. To save our analysis from unessentials, extraneous details such as orbital motion, gravitational forces, gyroscopic forces due to momentum wheels or control moment gyros, damping, and so on are ignored.

The displacement $w(x,y,t)$ at any point $P(x,y) \in \mathcal{V}$ is given by (see Hughes[6])

$$w(x,y,t) = z_c(t) + y\theta_x(t) - x\theta_y(t) + \begin{cases} 0 & P \in \mathcal{R} \\ u(x,y,t) & P \in \mathcal{E} \end{cases} \quad (1)$$

Only linear (z_c,θ_x,θ_y) and small deformation u are relevant here. The equations of motion for z_c,θ_x,θ_y,u, and the boundary conditions associated with u are derived by invoking Hamilton's principle on the following energy expressions

$$2T = m_r\dot{z}_c^2 + I_{rx}\dot{\theta}_x^2 + I_{ry}\dot{\theta}_y^2 + \mu\int_{\mathcal{E}} \dot{w}^2(x,y,t)\,dA \quad (2)$$

$$2U = D\int_{\mathcal{E}} \{(\Delta^2 w)^2 - 2(1-\nu)\Delta w\}\,dA \quad (3)$$

$$\Delta w \triangleq w_{,xx}w_{,yy} - (w_{,xy})^2 \qquad \Delta^2 w = w_{,xx} + w_{,yy} \quad (4)$$

where T is kinetic energy and U is strain energy.

For partial differentiation the comma notation is employed in Eq. (4) and throughout. In the absence of any forces the governing equations are deduced to be

$$m\ddot{z}_c + \mu\int_{\mathcal{E}} \ddot{u}\,dA = 0 \quad (5a)$$

$$I_{xx}\ddot{\theta}_x + \mu\int_{\mathcal{E}} y\ddot{u}\,dA = 0 \quad (5b)$$

$$I_{yy}\ddot{\theta}_y - \mu\int_{\mathcal{E}} x\ddot{u}\,dA = 0 \quad (5c)$$

$$D\nabla^4 u + \mu(\ddot{z}_c + y\ddot{\theta}_x - x\ddot{\theta}_y + \ddot{u}) = 0 \quad (5d)$$

where ∇^4 is a biharmonic operator and

$$m = m_r + m_e \qquad I_{xx} = I_{rx} + I_{ex} \qquad I_{yy} = I_{ry} + I_{ey} \quad (6)$$

The following boundary conditions, associated with Eq. (5), are those for a free rectangular plate:

$$u_{,xx} + \nu u_{,yy} = 0 \qquad u_{,xxx} + (2-\nu)u_{,xyy} = 0 \qquad x = \pm a/2 \quad (7a)$$

$$u_{,yy} + \nu u_{,xx} = 0 \qquad u_{,yyy} + (2-\nu)u_{,xxy} = 0 \qquad y = \pm b/2 \quad (7b)$$

$$u_{,xy} = 0 \qquad x = \pm a/2 \qquad y = \pm b/2 \quad (7c)$$

These conditions will not be utilized here; they have been recorded for completeness. Since external forces are not relevant in this paper, they are not considered above; however, the interested readers may consult Ref. 12 for modeling of distributed and point moments and forces. For

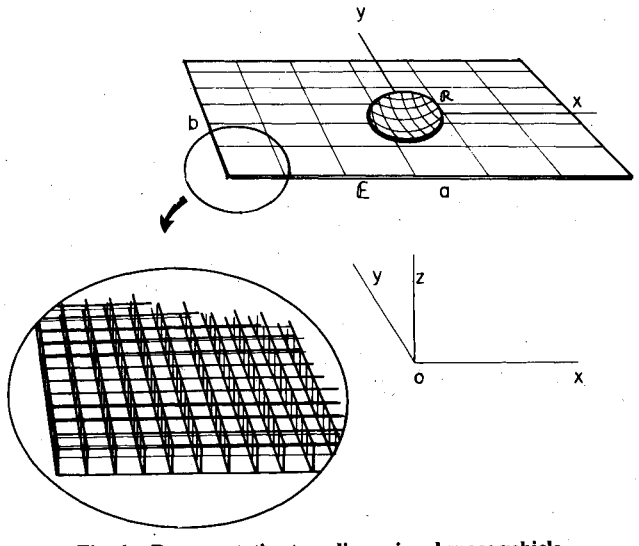

Fig. 1 Representative two-dimensional space vehicle.

future reference, the linear and angular momentum of the vehicle are noted below:

$$p \triangleq \int_{\nabla} \dot{w} dm = m\dot{z}_c + \int_{\mathcal{E}} \dot{u} dm \tag{8a}$$

$$h_x \triangleq \int_{\nabla} y\dot{w} dm = I_{xx}\dot{\theta}_x + \int_{\mathcal{E}} y\dot{u} dm \tag{8b}$$

$$h_y \triangleq -\int_{\nabla} x\dot{w} dm = I_{yy}\dot{\theta}_y - \int_{\mathcal{E}} x\dot{u} dm \tag{8c}$$

where dm is elemental mass. The reader should note the difference between $w\ (x,y,t)$ and $u\ (x,y,t)$; the former is the displacement of any point on ∇ in the inertial triad $(oxyz)$ whereas the latter is the elastic deformation of $\mathcal{E}$ in the rigid-body-embedded-triad such that at the $\mathcal{R}/\mathcal{E}$ interface, which presently coincides with the mass center of both, the following is true:

$$u = u_{,x} = u_{,y} = 0$$
$$w = z_c \qquad w_{,y} = \theta_x(t) \qquad -w_{,x} = \theta_y \tag{9}$$

This difference carries over in modal analysis and takes on new implications which are deduced in the next section.

III. Modal Analysis

The deformation u is now expressed as a superposition of natural modes of vibrations. Several families of modes can be identified; only two sets of modes, the constrained and the unconstrained, will be discussed here. In the lineage of modes, as it will become apparent to the reader, the unconstrained modes are more accurate than the constrained modes. Consequently, the constrained modes will be discussed first.

A. Constrained Modes

Recall that the constrained modes describe a situation in which the rigid body is stationary. From Eq. (1) we note that for a motionless rigid body the distinction between w and u disappears and Eq. (5d) informs us that the constrained situation is governed by

$$D\nabla^4 u + \mu\ddot{u} = 0 \tag{10}$$

The natural frequency Ω_n and the nth constrained mode U_n satisfies, from Eq. (10),

$$D\nabla^4 U_n = \mu\Omega_n^2 U_n \qquad n \in \mathcal{S} \tag{11}$$

The boundary conditions, Eqs. (7), suitably modified, continue to apply for Eqs. (10) and (11). Note that $U_n(x,y)$, where $n \in \mathcal{S}$, is not an assumed mode.

When the natural motion of the spacecraft is written as a superposition of these modes,

$$u(x,y,t) = \Sigma_n U_n(x,y) Q_n(t) \qquad \Sigma_n = \sum_{n=1}^{\infty} \tag{12}$$

the motion equations (5) can be reduced by standard techniques to

$$m\ddot{z}_c + \Sigma_n P_n \ddot{Q}_n = 0,$$

$$I_{xx}\ddot{\theta}_x + \Sigma_n H_{xn}\ddot{Q}_n = 0 \qquad I_{yy}\ddot{\theta}_y + \Sigma_n H_{yn}\ddot{Q}_n = 0$$

$$P_n\ddot{z}_c + H_{xn}\ddot{\theta}_x + H_{yn}\ddot{\theta}_y + \ddot{Q}_n + \Omega_n^2 Q_n = 0, \qquad n \in \mathcal{S} \tag{13}$$

where

$$P_n \triangleq \int_{\mathcal{E}} U_n dm \quad H_{xn} \triangleq \int_{\mathcal{E}} yU_n dm \quad H_{yn} \triangleq -\int_{\mathcal{E}} xU_n dm \quad n \in \mathcal{S} \tag{14}$$

and the orthonormality condition is

$$\int_{\mathcal{E}} U_n U_m dm = \delta_{nm} \text{ (Kronecker delta)} \qquad n,m \in \mathcal{S} \tag{15}$$

The P_n are called the "modal momentum coefficients"; and (H_{xn}, H_{yn}) the "modal angular momentum coefficients"; Likins[3] calls these parameters (except for sign) the "flexibility influence coefficients";

Hughes[2,6] has shown that the coefficients, Eq. (14), satisfy certain identities. Applied to the present vehicle, these become

$$\Sigma_n P_n^2 = m_e \qquad \Sigma_n H_{xn}^2 = I_{ex} \qquad \Sigma_n H_{yn}^2 = I_{ey} \tag{16a}$$

$$\Sigma_n H_{xn} P_n = 0 \qquad \Sigma_n H_{yn} P_n = 0 \qquad \Sigma_n H_{xn} H_{yn} = 0 \tag{16b}$$

The identities can be normalized such that the right sides in Eq. (16a) are unity. We note that while deriving the identities it is assumed that an infinite number of exact constrained eigenfunctions are available. However, due to discretization, we only have a finite number of approximate eigenfunctions. Hughes and Skelton[13] define "completeness indexes" $\mathcal{I}_c(N)$ of the form

$$\mathcal{I}_c(N) \triangleq (\hat{P}_n^2, \hat{H}_{xn}^2, \hat{H}_{yn}^2) \tag{17}$$

Hence, a complete model yields $\mathcal{I}_c(\infty) = 1$. Clearly, $\mathcal{I}_c(N)$ is a measure of the truncation error when N constrained modes are retained. We will carefully analyze the utility of $\mathcal{I}_c(N)$ in Sec. V.E.

To emphasize the additional usefulness of P_n, H_{xn}, H_{yn}, $n \in \mathcal{S}$, we observe that the control designs employing the hybrid coordinate approach due to Likins[3] retain the modes based on these coefficients, Larson et al.[14] for example. The reader may have noticed that Eq. (13) is a coupled system equivalent to Eq. (279) in Ref. 3; and a transformation is still needed for decoupling. On the other hand, discretization as well as decoupling can be achieved at once if one employs the unconstrained modes. This is done next.

Table 1 Natural frequency of a uniform rectangular flat plate

Mode α	N_e	σ = 1	σ = 1.5	σ = 2.5
4	1	13.6601	20.3680	25.5667
	4	13.5727	20.2423	21.5037
	16	13.4773	20.1092	21.4779
	L[a]	13.4890	20.1280	21.6430
5	1	22.4499	25.3251	33.3077
	4	19.6354	21.4628	33.1612
	16	19.6133	21.4361	33.0102
	L	19.7890	21.6030	33.0500
6	1	30.5941	52.4650	82.0252
	4	24.3485	46.8662	67.8320
	16	24.3053	46.4882	60.0022
	L	24.4320	46.6540	60.1370
7	1	39.2347	61.0216	87.0850
	4	35.1175	50.0623	71.6655
	16	34.8857	49.9756	71.0549
	L	35.0240	50.2930	71.4840
8	1	39.2347	69.5164	154.6741
	4	35.1175	61.3100	126.1279
	16	34.8857	57.9652	117.3308
	L	35.0240	58.2010	117.4500
9	1	80.4984	95.7372	167.9027
	9	64.7343	72.4037	136.0162
	16	61.4911	67.3164	119.3538
	L	61.5260	67.4940	119.3800

[a] Results due to Leissa.[16]

B. Unconstrained Modes

Since the vehicle in this situation is free to vibrate, the following expansion of the motion variables $(z_c,\theta_x,\theta_y,u)$ is natural

$$\begin{bmatrix} z_c(t) \\ \theta_x(t) \\ \theta_y(t) \\ u(x,y,t) \end{bmatrix} = \begin{bmatrix} z_{c1}\eta_1 \\ \theta_{x2}\eta_2 \\ \theta_{y3}\eta_3 \\ 0 \end{bmatrix} + \Sigma_\alpha \begin{bmatrix} z_{c\alpha} \\ \theta_{x\alpha} \\ \theta_{y\alpha} \\ u_\alpha(x,y) \end{bmatrix} \eta_\alpha(t)$$

$$\Sigma_\alpha = \sum_{\alpha=4}^{\infty} \qquad (18)$$

Equation (18) should be compared with Eq. (12). The differences are as follows. Included in the above expansion are the zero-frequency modal coordinates η_1,η_2,η_3 whose corresponding mode shapes consist of the uniform translation along the z and the rotations about the x and y axis, respectively. These are called the rigid modes; comments of Likins on p. 64 of Ref. 3 are valuable (he does not formulate the unconstrained modes though). We feel strange to note that despite the evident naturalness—and the consequent usefulness—we have not encountered expansions such as Eq. (18) in the literature on spacecraft dynamic analysis, except in the writings of Hughes,[6] for example.

The modal coordinates $\eta_\alpha,\alpha\in\mathcal{S}_e$ correspond to the "unconstrained-vehicle mode" ("unconstrained mode" for short) $w_\alpha,\alpha\in\mathcal{S}_e$ which is defined as

$$w_\alpha(x,y) = z_{c\alpha} + y\theta_{x\alpha} - x\theta_{y\alpha} + \begin{cases} 0 & (x,y)\in\mathcal{R} \\ u_\alpha(x,y) & (x,y)\in\mathcal{E} \end{cases} \qquad (19)$$

Equation (19) is parallel to Eq. (1). In Eqs. (18) and (19) the $(z_{c\alpha},\theta_{x\alpha},\theta_{y\alpha})$ are metric of participation of $\mathcal{R}$ in $w_\alpha,\alpha\in\mathcal{S}_e$. The $u_\alpha,\alpha\in\mathcal{S}_e$, which may be called "unconstrained-structure mode," satisfies

$$D\nabla^4 u_\alpha = \mu\omega_\alpha^2(z_{c\alpha} + y\theta_{x\alpha} - x\theta_{y\alpha} + u_\alpha) \qquad (20)$$

and the boundary conditions, Eqs. (7), modified appropriately. Since the linear and angular momentum associated with any unconstrained mode $w_\alpha,\alpha\in\mathcal{S}_e$ is zero, the following relations between $z_{c\alpha},\theta_{x\alpha},\theta_{y\alpha}$ and u_α from Eqs. (8) can be deduced.

$$-mz_{c\alpha} = p_\alpha = \mu\int_{\mathcal{E}} u_\alpha \mathrm{d}A \qquad -I_{xx}\theta_{x\alpha} = h_{x\alpha} = \mu\int_{\mathcal{E}} yu_\alpha \mathrm{d}A$$

$$-I_{yy}\theta_{y\alpha} = h_{y\alpha} = -\mu\int_{\mathcal{E}} xu_\alpha \mathrm{d}A \qquad \alpha\in\mathcal{S}_e \qquad (21)$$

Like (P_n,H_{xn},H_{yn}) in Eq. (14), the p_α are called the "modal momentum coefficients" and the $h_{x\alpha},h_{y\alpha}$ are the "modal angular momentum coefficients" associated with the mode u_α in the unconstrained mode w_α.

While looking back the reader will note that $U_n n\in\mathcal{S}$ in Eq. (11) is generally not the same as $u_\alpha,\alpha\in\mathcal{S}_e$ in Eq. (20). However, when the rigid body does not participate in the unconstrained mode w_α, even though allowed to, that is, when $z_{c\alpha}=\theta_{x\alpha}=\theta_{y\alpha}=0$ for αth mode, then u_α and the corresponding U_n become the same. Examples of such "noninteractive modes" will be found in Sec. IV.D. Though with the aid of Eq. (19), Eq. (20) can be written as

$$D\nabla^4 w_\alpha = \omega_\alpha^2 w_\alpha \qquad \alpha\in\mathcal{S}_e \qquad (22)$$

only in Eq. (20) the interaction between the rigid body motion and the elastic deformation is transparent. The orthonormality conditions obeyed by $w_\alpha,\alpha\in\mathcal{S}$ are

$$mz_{c1}^2 = 1 \qquad I_{xx}\theta_{x2}^2 = 1 \qquad I_{yy}\theta_{y2}^2 = 1 \qquad (23a)$$

$$\int_{\mathcal{E}} u_\alpha w_\beta \mathrm{d}m = \delta_{\alpha\beta} \qquad \int_{\mathcal{V}} w_\alpha w_\beta \mathrm{d}m = \delta_{\alpha\beta} \qquad (23b)$$

$$\int_{\mathcal{E}} u_\alpha D\nabla^4 u_\beta \mathrm{d}A = \omega_\alpha^2\delta_{\alpha\beta}$$

$$\int_{\mathcal{E}} u_\alpha u_\beta \mathrm{d}m - (mz_{c\alpha}z_{c\beta} + I_{xx}\theta_{x\alpha}\theta_{x\beta} + I_{yy}\theta_{y\alpha}\theta_{y\beta}) = \delta_{\alpha\beta} \quad \alpha,\beta\in\mathcal{S}_e \qquad (23c)$$

These conditions should be compared with the conditions of Eq. (15). The reader should note the domains of integration in Eqs. (15) and (23). Employing the foregoing preliminaries, the vehicle equations of motion (5) can eventually be transformed to

$$\text{Rigid modes:} \qquad mz_{c1}\ddot{\eta}_1 = 0, \quad I_{xx}\theta_{x2}\ddot{\eta}_2 = 0, \quad I_{yy}\theta_{y3}\ddot{\eta}_3 = 0$$

$$\text{Elastic modes:} \qquad \ddot{\eta}_\alpha + \omega_\alpha^2\eta_\alpha = 0, \quad \alpha\in\mathcal{S}_e \qquad (24)$$

As anticipated, unlike Eq. (13), Eqs. (24) are uncoupled. The unconstrained coefficients $(p_\alpha,h_{x\alpha},h_{y\alpha}\alpha\in\mathcal{S}_e)$, similar to the constrained coefficients $(P_n,H_{xn},H_{yn},n\in\mathcal{S})$ satisfy the following identities[6]:

$$\Sigma_\alpha p_\alpha^2 = m_e m/m_r \qquad \Sigma_\alpha h_{x\alpha}^2 = I_{ex}I_{xx}/I_{rx} \qquad \Sigma_\alpha h_{y\alpha}^2 = I_{ey}I_{yy}/I_{ry} \qquad (25a)$$

$$\Sigma_\alpha p_\alpha h_{x\alpha} = 0 \qquad \Sigma_\alpha p_\alpha h_{y\alpha} = 0 \qquad \Sigma_\alpha h_{x\alpha}h_{y\alpha} = 0 \qquad (25b)$$

Comparing the "unconstrained" identities of Eqs. (25) with the "constrained" identities of Eqs. (16), we learn that the former involve inertia properties of both $\mathcal{R}$ and $\mathcal{E}$, whereas the latter contain properties of $\mathcal{E}$ only. Implications of this difference will be examined in detail in Sec. IV.

Normalization of Eq. (25a) leads to the following "unconstrained completeness indexes" suggested in Ref. 13:

$$\mathcal{I}_u(N) = \Sigma_\alpha(\hat{p}_\alpha^2, \hat{h}_{x\alpha}^2, \hat{h}_{y\alpha}^2) \qquad (26)$$

This may be compared with $\mathcal{I}_c(N)$ defined in Eq. (17). Subsequently, the reader will discover that the $\mathcal{I}_u(N)$ are more incisive indexes of the truncation error than are the $\mathcal{I}_c(N)$.

With the uncoupled equations (24), the immediate objective of this section has been achieved.

IV. Numerical Results and Discussion

In this section we determine the eigenfunctions $U_n,n\in\mathcal{S}$, $w_\alpha,\alpha\in\mathcal{S}_e$, the modal coefficients $(P_n,H_{xn},H_{yn}),n\in\mathcal{S}$ and $(p_\alpha,h_{x\alpha},h_{y\alpha}),\alpha\in\mathcal{S}_e$, and examine the growth pattern of the completeness indexes $\mathcal{I}_c(N)$, $\mathcal{I}_u(N)$. This is done for a wide range of $\mathcal{R}/\mathcal{E}$ inertia ratios at different levels of discretization.

A. Computational Strategy

A closed-form solution of Eqs. (11) and (22) with the suitably modified boundary conditions of Eqs. (7) does not seem accessible; finite-element method, however, can handle this problem efficiently.

For discretization $w(x,y,t)$ is expressed as a product of the spatial bicubic Hermite polynomials and the temporal nodal variables (see Bogner et al.[15]).† In the present case, the finite

†Guidance of Prof. H.T.Y. Yang at this stage is gratefully acknowledged.

element is a rectangle having node at each corner; each node having four variables.

The element stiffness and mass matrices are obtained from the energy expressions, Eqs. (2) and (3); these two symmetric 16×16 matrices, recorded in Ref. 15 are verified by us. The rigid body at the center of the spacecraft is included by always having a node at the center of the platform. The discrete motion equations are:

$$\mathfrak{M}\ddot{q}+\mathfrak{K}q=0 \tag{27}$$

which is yet another, and more familiar to the technical community, discrete version of Eq. (5). For a 16-element approximation both $\mathfrak{M}$ and $\mathfrak{K}\in\mathfrak{R}^{100\times100}$, the entries of $q\in\mathfrak{R}^{100}$ are the nodal variables. As all the boundary conditions of Eqs. (7) are natural, and the shape function contains the three rigid modes already mentioned, $\mathfrak{K}$ is singular having zero eigenvalue of multiplicity three. The equations for the constrained dynamics are obtained by deleting the elements (z_c,θ_x,θ_y) from q and the corresponding rows and columns from the matrices $\mathfrak{M}$ and $\mathfrak{K}$ in Eq. (27). The constrained modes $U_n n\in\bar{\mathfrak{S}}$ can be constructed by multiplying the constrained eigenvectors with the shape function. Computation of the constrained modal coefficients P_n, $H_{xn},H_{yn}n\in\bar{\mathfrak{S}}$ in Eq. (14) follows.

The unconstrained dynamics is accessible via two routes. By substituting P_n,H_{xn},H_{yn}, $n\in\mathfrak{S}_N$ in Eq. (13) the unconstrained eigenvectors, the mode shapes u_α, the coefficients $p_\alpha,h_{x\alpha}$, $h_{y\alpha}$, $\alpha\in\mathfrak{S}_{eN}$ of varying accuracy can be computed by choosing different N. One may, instead, directly consider a 100×100 eigenvalue problem associated with Eq. (27) and compute u_α, p_α, $h_{x\alpha}$, $h_{y\alpha}$, $\alpha\in\bar{\mathfrak{S}}_e$. Here, the latter approach, which is more accurate, is employed. Also, the accuracy of the former approach is checked with the latter in Sec. IV.E.

B. Verification of Computations

The predicted natural frequencies of a free uniform isotropic plate are compared with those given by Leissa.[16] Leissa obtains his results by applying the Rayleigh-Ritz method while using 36 beam functions, six in each of the two directions. When the mass and inertia of $\mathfrak{R}$ are set to zero, the spacecraft model becomes equivalent to a completely free rectangular flat plate. The comparison with Ref. 16 is shown in Table 1 whose entries are the nondimensional frequencies $\bar{\omega}_\alpha$ $(\alpha=4,\ldots,9)$. Evidently, the 4-element approximation (36×36 matrices) predicts the lowest two frequencies for the range $1\le\sigma\le2.5$ nearly as accurately as 36 beam functions do. The 16-element approximation yields results that are more accurate than those already available in the literature.

Having assessed the accuracy of the computations, we next examine the distribution of the modal coefficients. In the remaining computations a space vehicle with $\sigma=2.5$ is chosen; it is modeled by 16 elements with the rigid body at the central node.

C. Constrained Modal Coefficients

Since $\mathfrak{R}$ is constrained to be motionless, the coefficients do not depend on its inertia properties. It turns out that due to symmetry of the plate which is constrained at the center, one, at most, of P_n, H_{xn}, H_{yn},$n\in\mathfrak{S}$ is nonzero. Thus the constrained modes are categorized into the following four classes:

$P_r\neq0$: $r=2, 5, 9, 11, 15, 17, 24, 28, 31, 34, 35, 41, 42, 53, \ldots$ (28a)

$H_{xs}\neq0$: $s=3, 7, 12, 18, 20, 22, 27, 33, 37, 45, 47, 49, 52, 57, \ldots$ (28b)

$H_{yt}\neq0$: $t=1, 6, 10, 13, 16, 21, 26, 30, 32, 36, 38, 43, 44, 54, \ldots$ (28c)

$P_l=H_{xl}=H_{yl}=0$: $l=4, 8, 14, 17, 18, 19, 23, 25, 29, 39, 40, 46, 48, 50, 51, \ldots$ (28d)

where the mode numbering is according to the ascending order of the constrained frequency. We nondimensionalize these coefficients as:

$$\tilde{P}_n=P_n/\mu_f \quad \tilde{H}_{xn}=H_{xn}/b'\mu_f \quad \tilde{H}_{yn}=H_{yn}/a'\mu_f \quad n\in\mathfrak{S} \tag{29}$$

Variation of P_n,H_{xn},H_{yn} against $n\in\bar{\mathfrak{S}}$ is shown in Fig. 2. We observe that generally these coefficients reduce rather rapidly with frequency. To obtain the dimensional value, the data in Eq. (31) below may be used.

As an additional, but important, observation, we note that Eqs. (28) decouple Eq. (13) into four sets and any set irrelevant to the control objective may be deleted with impunity. For instance, if we are concerned with the attitude control of $\mathfrak{R}$, only the modes having H_{xs} and H_{yt} need be considered. Stated differently, let Q_c, Q_x, Q_y, and Q_0 be the modal coordinates associated with the modes in Eqs. (28a), (28b), (28c) and (28d), respectively. If y is the controlled variable, then for the attitude control y is a function only of

$$y=[\theta_x Q_x^T\theta_y Q_y^T]^T \tag{30}$$

Due to the absence of the coupling the modes in Eqs. (28a) and (28d) are output unobservable, hence, truncatable. Expansion of these ideas can be reviewed in Refs. 4, 13, 17, and 18.

D. Unconstrained Modal Coefficients

Now we must choose inertia ratios between $\mathfrak{R}$ and $\mathfrak{E}$ and the size of $\mathfrak{E}$. A space vehicle with the following parameters

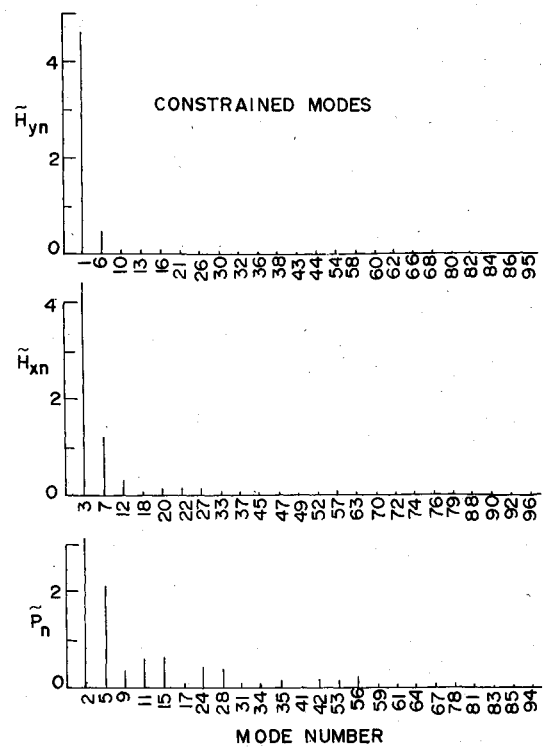

Fig. 2 Distribution of constrained modal coefficients.

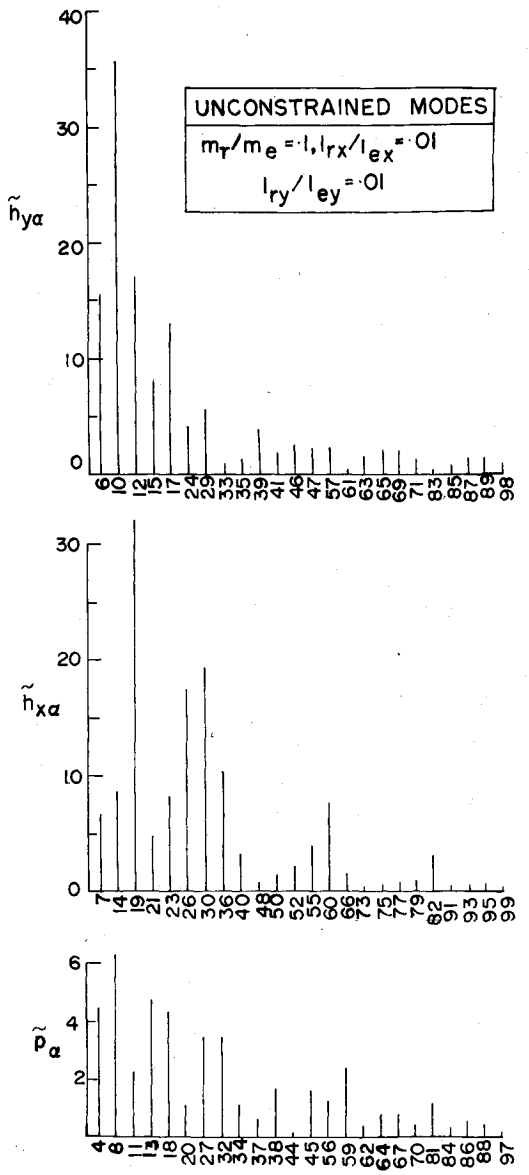

Fig. 3 Distribution of unconstrained modal coefficients—I.

represents a wide range of future large space structures:

$$m_r/m_e = 0.1 \quad I_{rx}/I_{ex} = I_{ry}/I_{ey} = 0.01 \quad \nu = 0.3 \quad \sigma = 2.5 \tag{31a}$$

$$a = 12.5\text{ km} \quad b = 5.0\text{km} \quad D = 20 \times 10^8 \text{NM} \quad \mu = 0.2622\text{ kg/m}^2 \tag{31b}$$

Table 2 shows the associated first hundred natural frequencies (rad/s). The three rigid modes preceding the vibrational modes have zero frequency. Figure 3 shows $\tilde{p}_\alpha$, $\tilde{h}_{x\alpha}$, $\tilde{h}_{y\alpha}, \alpha \in \bar{\mathcal{S}}_e$ for the ratio Eq. (31a) where

$$\tilde{p}_\alpha = p_\alpha/\mu_f \quad \tilde{h}_{x\alpha} = h_{x\alpha}/b'\mu_f \quad \tilde{h}_{y\alpha} = h_{y\alpha}/a'\mu_f \quad \alpha \in \bar{\mathcal{S}}_e \tag{32}$$

It is observed that similar to the constrained dynamic one, at most, of p_α, $h_{x\alpha}$, $h_{y\alpha}$, $\alpha \in \bar{\mathcal{S}}_e$ is nonzero. Indeed from Fig. 3 we determine four classes of modes for the ratios, Eq. (31a); consequently, Eq. (24), a system of 100 uncoupled second-order equations, is split into four sets each with 25 equations. The four sets of modes are as follows.

$$p_\beta \neq 0: \quad \beta = 4, 8, 11, 13, 18, 20, 27, 32, 34, \ldots \tag{33a}$$

$$h_{x\gamma} \neq 0: \quad \gamma = 7, 14, 19, 21, 23, 26, 30, 36, 40, \ldots \tag{33b}$$

$$h_{y\delta} \neq 0: \quad \delta = 6, 10, 12, 15, 17, 24, 29, 33, 35, \ldots \tag{33c}$$

$$p_\epsilon = h_{x\epsilon} = h_{y\epsilon} = 0: \quad \epsilon = 5, 9, 16, 22, 25, 28, 31, 42, 43, 49, \ldots \tag{33d}$$

The magnitude of $\tilde{p}_\alpha$, $\tilde{h}_{x\alpha}$, $\tilde{h}_{y\alpha}$, $\alpha \in \bar{\mathcal{S}}_e$ is somewhat closer to the magnitudes of P_n, H_{xn}, $H_{yn}, n \in \bar{\mathcal{S}}$; compare Figs. 2 and 3. However, the reader is alerted not to draw conclusions quickly. A great deal of attention will be devoted to the magnitude aspect shortly.

Zeroness or nonzeroness of p_α, $h_{x\alpha}$, $h_{y\alpha}, \alpha \in \bar{\mathcal{S}}_e$ depends on the symmetry and antisymmetry of the mode, or, equivalently, on the interactional coefficient $z_{c\alpha}$, $\theta_{x\alpha}$, $\theta_{y\alpha}, \alpha \in \bar{\mathcal{S}}_e$. To recognize this, Fig. 4 may be related to Table 3. Figure 4 records the nodal lines of 30 modes for the spacecraft, Eqs. (31). The nodal lines are obtained by representing the structure by a very fine mesh and by using first-order interpolation. Displacement at any point of the mode less than 10^{-6} is taken to be zero. Further characterization of the modes is done in Table 3. The reader is reminded that due to the three rigid modes the mode 4 is, in fact, the first elastic mode, and so on. Examining the nature of the modes, we note that the mode 28, for instance, in Fig. 4 is antisymmetric about both the x and y axis. Consequently, they do not induce any motion in the rigid body; in Sec. III.B. such modes are called noninteractive modes. These belong to the subset Eq. (33d), labeled as class 4 in Table 3. Poelaert[8,9] and Kabamba[19] call them "local mode." They are, in fact, the same as the fourth subset of the constrained modes in Eq. (28d). The mode numbers will not be the same because interspersions of the two subsets differ. Furthermore, as shown in Table 3, if the shape of $\mathcal{E}$ is to be controlled, these modes deserve consideration; however, for the attitude control or stationkeeping they can be truncated with no errors.

The mode 57 with frequency 1.0532 rad/s is included in Fig. 4 to show how ruffled the structure becomes by the excitation of such higher modes. (It is recognized that linearization may fail for such high modes.)

Regarding the remaining three classes of modes, Eqs. (33a-c), we note that the method that can determine the coefficients $z_{c\alpha}$, $\theta_{x\alpha}$, $\theta_{y\alpha}$ without asking for the eigenfunction $u_\alpha, \alpha \in \bar{\mathcal{S}}_e$ is desired because the determination of $u_\alpha(x,y), \alpha \in \bar{\mathcal{S}}_e$ to compute p_α, $h_{x\alpha}$, $h_{y\alpha} \alpha \in \bar{\mathcal{S}}_e$ is expensive. Poelaert[8,9] has suggested the receptance method to this end; of course, these methods ignore the noninteractive modes.

Due to their importance, some readers may wish to savor the numerical flavor of the coefficients $z_{c\alpha}, \theta_{x\alpha}, \theta_{y\alpha}, \alpha \in \bar{\mathcal{S}}_N (N = 100)$; this is reported in Ref. 20.

It is revealing to know the distribution of p_α, $h_{x\alpha}$, $h_{y\alpha}, \alpha \in \bar{\mathcal{S}}_e$ for a light, rigid body such as

$$m_r/m_e = 0.05 \quad I_{rx}/I_{ex} = 0.0001 \quad I_{ry}/I_{ey} = 0.0001 \tag{34}$$

The associated coefficients are shown in Fig. 5. Comparing the "constrained" distribution (Fig. 2) with the "unconstrained" distribution (Fig. 5), we learn that the two distributions are significantly different. This is because the constrained dynamics is a limiting case of a space structure having $\mathcal{R}$ of infinite inertia so that the elastic deformations fail to shake it. On the other hand, when $\mathcal{R}$ is as light as in Eqs. (34), p_α, $h_{x\alpha}$, $h_{y\alpha}$ form a slowly decreasing oscillatory series. Several complications will be noted in the next section.

Having examined the properties of the modal coefficients, we now focus on the modal identities and the completeness indexes associated with both types of modes.

E. Completeness Indexes and Truncation Errors

P_n, H_{xn}, H_{yn}, $n \in \bar{\mathcal{S}}$ are computed in Sec. IV.C. Using these, the $\mathcal{I}_c(N)$, Eq. (17), which are unity for $N = \infty$ are found to be, for $N = 97$,

$$\mathcal{I}_c(97) = (0.9789, 0.9997, 0.9997) \tag{35}$$

Table 2 Natural frequencies of a representative space vehicle

1	0	26	2.9099E−01	51	8.2942E−01	76	2.0338
2	0	27	2.9729E−01	52	8.5397E−01	77	2.0660
3	0	28	3.3112E−01	53	8.6868E−01	78	2.1929
4	1.1320E−02	29	3.4267E−01	54	9.3997E−01	79	2.4797
5	1.8447E−02	30	3.8783E−01	55	9.5891E−01	80	2.5341
6	3.1936E−02	31	3.9136E−01	56	1.0375	81	3.1148
7	3.9320E−02	32	3.9286E−01	57	1.0532	82	3.1506
8	5.8471E−02	33	4.2967E−01	58	1.1130	83	3.1603
9	6.6701E−02	34	4.3203E−01	59	1.1477	84	3.1651
10	7.2993E−02	35	4.8240E−01	60	1.1627	85	3.2037
11	7.6985E−02	36	4.9170E−01	61	1.2287	86	3.2347
12	9.0448E−02	37	4.9985E−01	62	1.2308	87	3.2868
13	9.9096E−02	38	5.0983E−01	63	1.2622	88	3.3716
14	9.9554E−02	39	5.2044E−01	64	1.2946	89	3.4258
15	1.3203E−01	40	5.3701E−01	65	1.3329	90	3.4885
16	1.5507E−01	41	5.6604E−01	66	1.4092	91	3.4897
17	1.6438E−01	42	5.6986E−01	67	1.4231	92	3.5353
18	1.7087E−01	43	5.8664E−01	68	1.4390	93	3.5467
19	1.8360E−01	44	6.4071E−01	69	1.4513	94	3.6318
20	1.8918E−01	45	6.5791E−01	70	1.8410	95	3.6733
21	2.1427E−01	46	6.6187E−01	71	1.8598	96	3.8019
22	2.2272E−01	47	7.2229E−01	72	1.8996	97	3.9308
23	2.3783E−01	48	7.8044E−01	73	1.9006	98	3.9609
24	2.5798E−01	49	7.8362E−01	74	1.9435	99	4.2036
25	2.8070E−01	50	8.1173E−01	75	1.9509	100	4.2496

Table 3 Four classes of unconstrained modes

Class	Modes kept for	About x axis	About y axis	$z_{c\alpha},\theta_{x\alpha},\theta_{y\alpha}$	$p_\alpha,h_{x\alpha},h_{y\alpha}$	Modes
1	SC or ACX	S	S	$z_{c\alpha}=\theta_{y\alpha}=0,\theta_{x\alpha}\neq 0$	$p_\alpha=h_{y\alpha}=0,h_{x\alpha}\neq 0$	7,14,...
2	SC or ACY	S	A	$z_{c\alpha}=\theta_{x\alpha}=0,\theta_{y\alpha}\neq 0$	$p_\alpha=h_{x\alpha}=0,h_{y\alpha}\neq 0$	6,10,...
3	SC or SK	S	S	$\theta_{x\alpha}=\theta_{y\alpha}=0,z_{c\alpha}\neq 0$	$h_{x\alpha}=h_{y\alpha}=0,p_\alpha\neq 0$	4,8,...
4	SC	A	A	$z_{c\alpha}=\theta_{x\alpha}=\theta_{y\alpha}=0$	$p_\alpha=h_{x\alpha}=h_{y\alpha}=0$	5,9,...

SC = shape control, ACX = attitude control about x axis, ACY = attitude control about y axis, SK = stationkeeping, A = antisymmetric, S = symmetric.

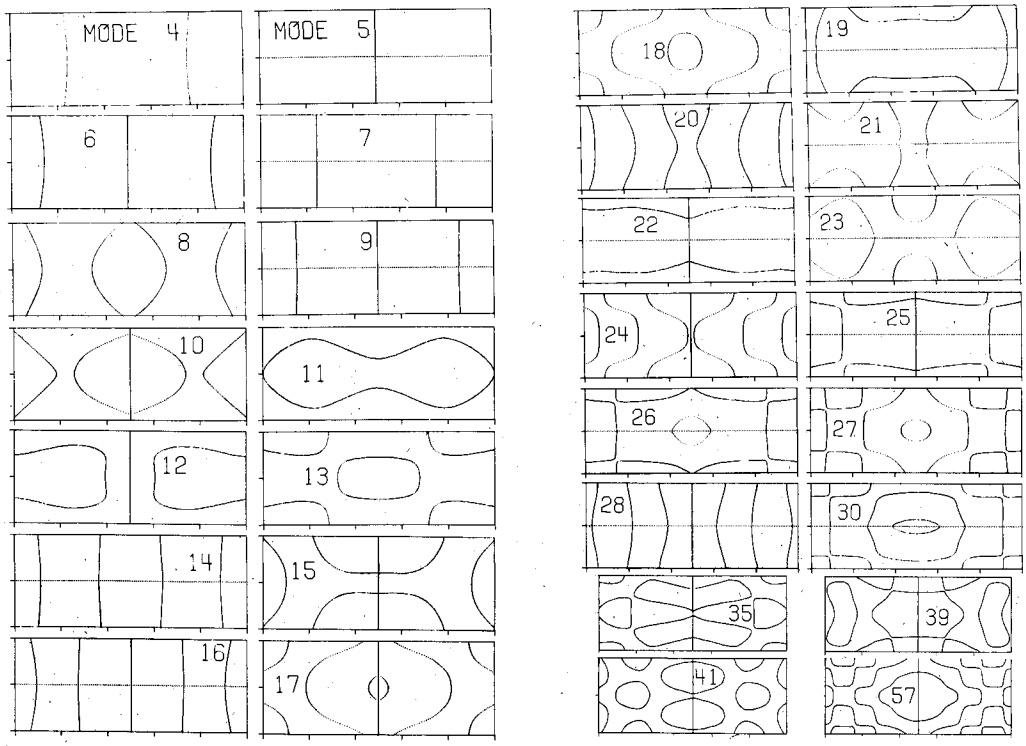

Fig. 4 Nodal patterns for a representative space vehicle.

respectively. The dashed lines in Figs. 6a-c (for the present, ignore the solid lines) show how $\mathcal{I}_c(N)$ grows as N increases. It is observed from Fig. 6b that the third constrained mode alone makes the model 92% complete with respect to H_{xn}. Similarly, from Fig. 6c we infer that the first constrained mode alone provides a model that is 98% complete with respect to H_{yn}. The identities, Eq. (16b), are valid because at least two of the P_n, H_{xn}, $H_{yn}, n\in\mathcal{S}$ are always zero. Thus, the identities, Eq. (16a) and P_n, H_{xn}, H_{yn}, guide us in deciding how many and which modes should be retained for a specified constrained inertial completeness.

Note that constrained dynamics describes only indirectly the $\mathcal{R}/\mathcal{E}$ interaction. Constrained coefficients P_n, H_{xn}, H_{yn} identify those appendage modes which should be retained to improve $\mathcal{I}_c$ for a given order of discrete model. When $\mathcal{R}$ is massive relative to $\mathcal{E}$, the unconstrained spacecraft modes, $u_\alpha\alpha\in\mathcal{S}_e$, are quite similar to the constrained modes, $U_n n\in\mathcal{S}$, because the structure-induced motion of $\mathcal{R}$ is slight. In such cases, it is plausible that $\mathcal{I}_c$ is a reliable indicator of the index $\mathcal{I}_u$. When $\mathcal{R}$ is light relative to $\mathcal{E}$, however, caution must be exercised in interpreting $\mathcal{I}_u$ from $\mathcal{I}_c$. The latter may, for instance, have to be 0.9999 to produce $\mathcal{I}_u$ of 0.90 for the unconstrained modes "deduced from them." This happens because small rigid bodies are easily tossed about by the neighboring elastic structure. To reinforce these comments we now examine the growth of $\mathcal{I}_u$ for the inertia ratios, Eq. (34) (see Fig. 6). The associated unconstrained modes of varying degree of accuracy are obtained by retaining the constrained modes—available from the 16-element approximation—in Eq. (13) from 3 to 97 in eleven steps.

It is observed from Fig. 6 that when 97 constrained modes are retained, the $\mathcal{I}_u$'s are

$$\Sigma_\alpha p_\alpha^2 = 0.6892 \quad \Sigma_\alpha h_{x\alpha}^2 = \Sigma_\alpha h_{hy\alpha}^2 = 0.2644 \quad \Sigma_\alpha = \sum_{\alpha=4}^{100} \tag{36}$$

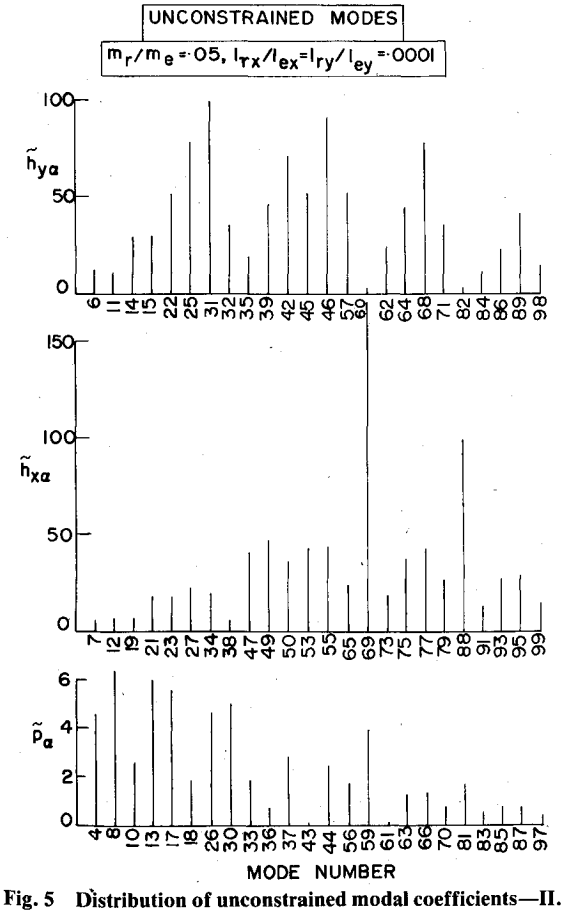

Fig. 5 Distribution of unconstrained modal coefficients—II.

These sums should be compared with those in Eq. (35) which do not depend on the inertia ratios. Evidently, the indexes, Eq. (36), are far less than unity, particularly for the angular momentum coefficients. Double precision computations are found to give results identical to Eq. (36) confirming that the error is in the initial truncation (16 are too few finite elements) not in the roundoff.

Figure 6 allows some very useful observations. The stairs of various heights in Fig. 6a suggest that in the case of the linear momentum the upper bounds to the p_α's are obtained if one retains only a few (say 3, 7, 17, ...) of the 97 constrained modes available from the 16-element approximation. The bounds monotonically approach the least upper bound as more of the constrained modes are retained for computing the unconstrained modes. A similar trend is observed in the case of the angular momentum about the x axis, as shown in Fig. 6b. Nevertheless, if the discretization is done by retaining fewer than 77 constrained modes, a "miscrediting" for the angular momentum (a false designation of $h_x \neq 0$) occurs as manifested by the spikes in Fig. 6b. The spikes signify that the "tail" (last) modes are miscredited with the angular momentum. For instance, when the retained "constrained" modes are 3, 7, 17, 27, 37, 57, or 67, the "unconstrained" tail modes which are miscredited with the x-angular momentum are 3rd, 7th, 17th, 27th, 37th, 57th, or 67th, respectively.

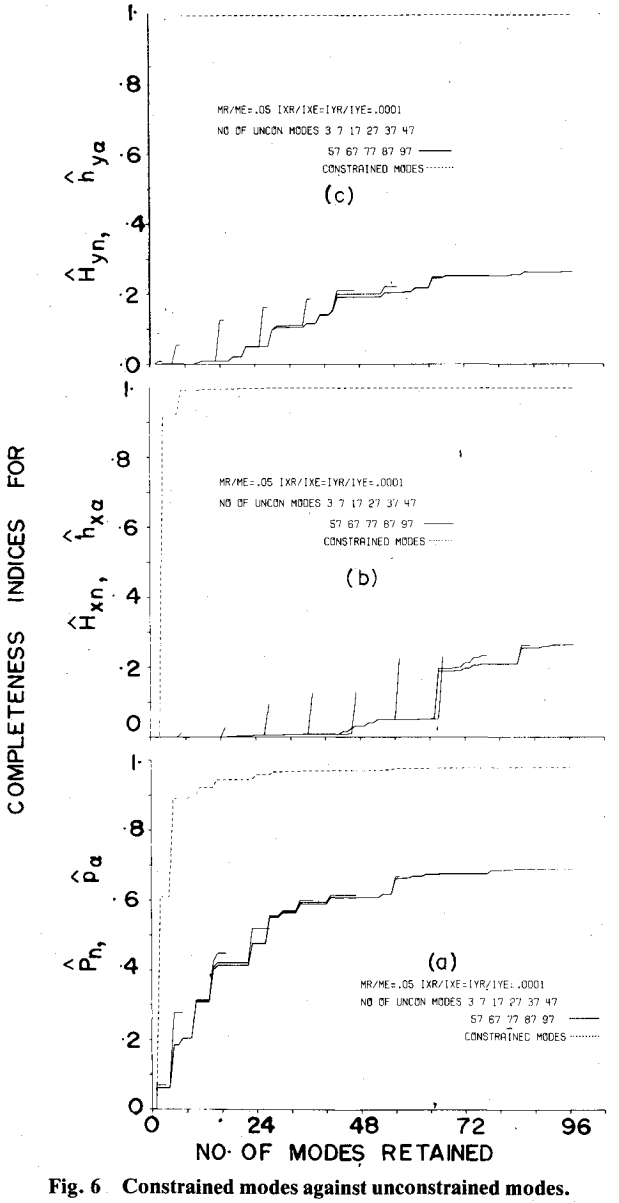

Fig. 6 Constrained modes against unconstrained modes.

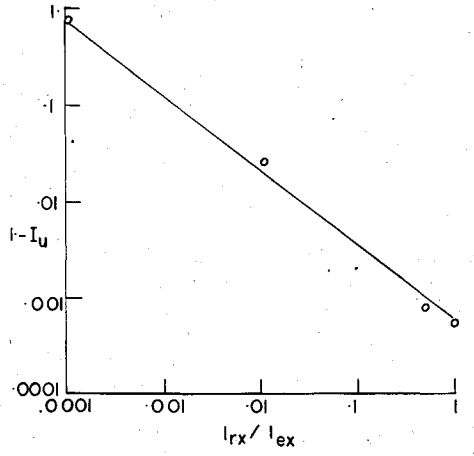

Fig. 7 Unconstrained completeness index against inertia ratio.

When the discretization is done by retaining 77 modes or more, the spikes disappear and the upper bounds of the $h_{x\alpha}$'s are instead obtained as in the case of the p_α's. Most of the discretization inaccuracy is contained in the "tail" modes and simply dropping them will enhance the accuracy of the discrete model. Meirovitch and Lindberg[21] report the frequencies having a similar trait (i.e., frequencies associated with the tail modes are excessively overpredicted). A plausible explanation is that when higher modes are being considered, the meaning of the phrase "small error in the constrained mode" has a very narrow latitude, and a very small error may indeed lead to substantially erroneous results. For more illumination, consult Ref. 7, p. 152.

Again, the spikes and the upper bounds are obtained in the case of the y-angular momentum also, though the miscrediting of the y-angular momentum vanishes when at least 37 constrained modes are retained. The miscredited "unconstrained" modes in this case are 2nd, 6th, 16th, or 26th when the "constrained" modes retained are 3, 7, 17, or 27, respectively. Finally, flat portions of the curves correspond to the modes with nil contributions. When the retained constrained modes are not adequate—in the sense that the miscrediting of the angular momentum persists, and if the number of modes having nonzero (P_n, H_{xn}, H_{yn}) are equal, the number of unconstrained modes having nonzero $(p_\alpha, h_{x\alpha}, h_{y\alpha})$ can be unequal.

The complicated dependence of the unconstrained modes on the constrained modes, unfolded above, helps decode the intriguing observations of Larson et al.[14] while designing a reduced-order optimal estimator for a solar electric propulsion spacecraft.

It is helpful to know the dependence of ϑ_u on the inertia ratios for a specified level of discretization. For the ratios, Eq. (31a), rewritten below, and the following two ratios

$$m_r/m_e = 0.1 \qquad I_{rx}/I_{ex} = I_{ry}/I_{ey} = 0.01 \tag{37a}$$

$$m_r/m_e = 1.0 \qquad I_{rx}/I_{ex} = I_{ry}/I_{ey} = 1.0 \tag{37b}$$

$$m_r/m_e = 1.0 \qquad I_{rx}/I_{ex} = I_{ry}/I_{ey} = 0.5 \tag{37c}$$

the indices, Eq. (26), are found to be

$$\vartheta_u(97) = (0.8089, 0.9726, 0.9726) \tag{38a}$$

$$\vartheta_u(97) = (0.9588, 0.9994, 0.9994) \tag{38b}$$

$$\vartheta_u(97) = (0.9588, 0.9991, 0.9991) \tag{38c}$$

respectively. Note that $\vartheta_u(97)$ in Eqs. (38b) and (38c) are as close to unity as are $\vartheta_c(97)$, [see Eq. (35)]. ϑ_u (97) for the y-angular momentum are plotted in Fig. 7. The relation is nearly a straight line.

Some comments about the related results available in the literature are in order. For illustrating the stationary principle for rotating structures, Meirovitch[22] considers a flexible spacecraft with inertia ratios (1/144, 1/360). Corresponding unconstrained frequencies are computed by admissible functions, nonrotating constrained modes, and rotating constrained modes. Though the frequencies are shown to be somewhat insensitive to the choice of the modes, we conjecture that the ϑ_u's associated with the rotating constrained modes are substantially better than with the admissible functions. A miscrediting in the tail modes obtained by using the admissible function is also noticeable in the data furnished.

Usefulness of $\vartheta_u(N)$ for truncating the modes is elaborated in Ref. 13. Some readers may be disturbed by $\vartheta_u(N) = 0.2644 \ll 1$ in Eq. (36) for the angular momentum. However, we observe that the modal coefficients and the completeness indices are only one of the means for reducing finite-element models. A truncation methodology needs to be based on a broader perspective such as the one opened by Refs. 4, 13, 18, 23, for example. From that viewpoint, $\vartheta_u = 0.2644$ becomes acceptable and we begin to perceive a wastefulness in computing still higher modes.

V. Concluding Remarks

The preceding gives a biopsy of motional interaction between the rigid body and the elastic structure in the case of a representative two-dimensional space vehicle. Implications of our findings for the modeling of flexible space structures are summed as follows:

1) The constrained modes contribute to the constrained modal identities almost according to frequency. Most of the contribution comes from the first few modes, the rest of the modes contribute negligibly. Unconstrained modes contributing most to the unconstrained completeness index tend to be less ordered by frequency.

2) The accuracy of an unconstrained and constrained modal expansion depends crucially on flexible/rigid inertia ratio. The number of modes required to achieve a specified value of the unconstrained completeness index increases with this ratio.

3) For a specified completeness index ϑ_u the unconstrained modes required will generally be fewer than the constrained modes. Thus, efforts to choose modes that have fewer constraints lead to a better completeness index; this happens because unconstrained modes contain better quality information.

4) When too few constrained modes are used, too much of the vehicle angular momentum is attributed to the tail modes, even though theoretically these modes may not have the momentum. As more constrained modes are retained, this error disappears.

5) The completeness indexes monotonically increase with the number of modes retained in the model.

In summary, we observe that the modal coefficients and the modal identities theorize the interfacial dynamics and are of great value in the process of order reduction.

Acknowledgments

We gratefully acknowledge numerous discussions at several stages of this work with Prof. P. C. Hughes, Institute for Aerospace Studies, University of Toronto and Prof. R. E. Skelton, School of Aeronautics and Astronautics, Purdue University. This research is funded by Jet Propulsion Laboratory under Contract 955639.

References

[1] Likins, P.W., "The New Generation of Dynamic Interaction Problems," *The Journal of the Astronautical Sciences,* Vol. 27, No. 2, April 1979, pp. 103-113.

[2] Hughes, P.C., "Dynamics of Flexible Space Vehicles with Active Attitude Control," *Celestial Mechanics,* Vol. 9, 1974, pp. 21-39.

[3] Likins, P.W., *Dynamics and Control of Flexible Space Vehicle,* IPL Technical Report, 32-1329, Rev. 1, Jan. 1970.

[4] Likins, P.W., Ohkami, Y., and Wong, C., "Appendage Modal Coordinate Truncation Criteria in Hybrid Coordinate Dynamic Analysis," *Journal of Spacecraft and Rockets,* Vol. 13, Oct. 1976, pp. 511-617.

[5] Margulies, G., Aubrun, J.N., Bushnell, D., and Ho, J.Y.L., "Multibody Flexible Spacecraft Integrated Analysis: Structures, Dynamics, and Controls," *Proceedings of the First VPI&SU/AIAA Symposium on Dynamics and Control of Large Flexible Spacecraft,* Blacksburg, Va., June 1977, pp. 437-456.

[6] Hughes, P.C., "Modal Identities for Elastic Bodies with Application to Vehicle Dynamics and Control," *Journal of Applied Mechanics,* Vol. 47, No. 1, March 1980, pp. 177-184.

[7] Bishop, R.E.D. and Johnson, D.C., *The Mechanics of Vibration,* Cambridge University Press, Cambridge, 1979.

[8] Poelaert, D.H., "Dynamic Analysis of a Nonrigid Spacecraft," *Proceedings of the First VPI&SU/AIAA Symposium on Dynamics and Control of Large Flexible Spacecraft,* Blacksburg, Va., June 1977, pp. 351-366.

[9] Poelaert, D.H., "A Distributed Element Technique for Dynamic Analysis of Flexible Space Structures," *Proceedings of the Second VPI&SU/AIAA Symposium on Dynamics and Control of Large Flexible Spacecraft,* Blacksburg, Va., June 1979, pp. 495-510.

[10] Noor, A.K., Anderson, M.S., and Greene, W.H., "Continuum Models for Beam and Plate-Like Lattice Structures," *AIAA Journal,* Vol. 16, Dec. 1978, pp. 1219-1228.

[11] Hablani, H.B., "Generic Model of a Large Flexible Space Structure for Control Concept Evaluation," *Journal of Guidance and Control,* Vol. 4, Sept.-Oct. 1981, pp. 558-561.

[12] Hablani, H.B., "A More Accurate Modeling of the Effects of Actuators in Large Space Structures," *Acta Astronautica,* Vol. 8, 1981, pp. 361-376.

[13] Hughes, P.C. and Skelton, R.E., "Modal Truncation for Flexible Spacecraft," *Journal of Guidance and Control,* Vol. 4, May-June 1981, pp. 291-297.

[14] Larson, V., Likins, P.W., and Marsh, E.L., "Optimal Estimation and Control of a Solar Electrical Propulsion Spacecraft," *IEEE Transactions on Aerospace and Electronic Systems,* Vol. 13, 1977, pp. 35-47.

[15] Bogner, F.K., Fox, R.L., and Schmit, L.A., "The Generation of Interelement Compatible Stiffness and Mass Matrices by the Use of Interpolation Formulas," *Proceedings of the 1st Conference on Matrix Methods in Structural Mechanics,* Wright Patterson AFB, Ohio, Nov. 1965.

[16] Leissa, A.W., "The Free Vibration of Rectangular Plates," *Journal of Sound and Vibration,* Vol. 31, No. 3, 1973, pp. 257-293.

[17] Hughes, R.C. and Skelton, R.E., "Controllability and Observability for Flexible Spacecraft," *Journal of Guidance and Control,* Vol. 3, Sept.-Oct. 1980, pp. 452-459.

[18] Skelton, R.E., Hughes, P.C., and Hablani, H.B., "Order Reduction for Models of Space Structures Using Modal Cost Analysis," communicated to *Journal of Guidance and Control.*

[19] Kabamba, P.T., "A Euclidean Approach to the Problem of Parameter Reduction in Large Systems," *Proceedings of the Second VPI&SU/AIAA Symposium on Dynamics and Control of Large Flexible Spacecraft,* Blacksburg, Va., June 1979, pp. 459-474.

[20] Hablani, H.B., *Dynamics and Control of a Large Two-Dimensional Flexible Spacecraft,* Purdue University, School of Aeronautics and Astronautics Technical Report, Aug. 1980.

[21] Meirovitch, L. and Lindberg, R., "A Global Ritz Method for Reduced Order Modeling of a Flexible Dish Antenna," *Proceedings of the Second VPI&SU/AIAA Symposium on Dynamics and Control of Large Flexible Spacecraft,* Blacksburg, Va., June 1979, pp. 209-235.

[22] Meirovitch, L., "A Stationary Principle for the Eigenvalue Problem for Rotating Structures," *AIAA Journal,* Vol. 14, Oct. 1976, pp. 1387-1394.

[23] Skelton, R.E., "Cost Decomposition of Linear Systems with Application to Model Reduction," *International Journal of Control* Vol. 32, No. 6, 1980, pp. 1031-1055.